JOURNAL OF GEOPHYSICAL RESEARCH, VOL. 113, D16S42, doi:10.1029/2007JD008833, 2008

Airborne Fourier transform spectrometer observations in support of EOS Aura validation

M. T. Coffey,[1] J. W. Hannigan,[1] A. Goldman,[2] D. Kinnison,[1] J. C. Gille,[1] J. J. Barnett,[3] L. Froidevaux,[4] A. Lambert,[4] M. Santee,[4] N. Livesey,[4] B. Fisher,[4] S. S. Kulawik,[4] and R. Beer[4]

Received 16 April 2007; revised 7 October 2007; accepted 28 November 2007; published 24 June 2008.

[1] Nearly coincident observations of HNO_3, HCl, N_2O, and H_2O in the vicinity of the northern polar vortex during the NASA Polar Aura Validation Experiment (PAVE) in January and February 2005 have shown reasonably good agreement between aircraft-borne infrared spectrometer results and results from High Resolution Dynamics Limb Sounder (HIRDLS), Microwave Limb Sounder (MLS), and Tropospheric Emission Spectrometer (TES) instruments aboard the EOS Aura satellite. Mixing ratio profile and column results show that special attention must be given to retrievals that may be disturbed by the dynamics and chemical processing of the polar vortex. Largest differences occur on days when observations were made in regions of the vortex with large gradients in wind and potential vorticity, and the differences were especially noticeable in results for HNO_3 and HCl, whose profiles may be dramatically changed by vortex activity. The mean difference between coincident column observations by MLS and the Fourier transform spectrometer (FTS) is 2.4%, VMR profile amounts generally are in good agreement between the satellite observations where they are available. The average difference between coincident HCl column observations by MLS and the FTS is 4.6%.

Citation: Coffey, M. T., et al. (2008), Airborne Fourier transform spectrometer observations in support of EOS Aura validation, *J. Geophys. Res.*, *113*, D16S42, doi:10.1029/2007JD008833.

1. Introduction

[2] During a recent, NASA-sponsored airborne campaign we deployed a high-resolution infrared spectrometer to measure total column amounts and mixing ratio vertical profiles of a number of gases also measured by instruments on the EOS Aura satellite. The main purpose of the Polar Aura Validation Experiment (PAVE) (http://cloud1.arc.nasa.gov/ave-polar/) was to provide coincident measurements of atmospheric gases and aerosols also measured by the four Aura experiments (HIRDLS, MLS, OMI, TES) (http://aura.gsfc.nasa.gov/), launched in July 2004. We report here measurements of gaseous constituents derived from the absorption of infrared solar radiation by the atmosphere above an aircraft platform. The NASA DC-8 aircraft was flown in January and February 2005, from a base in New Hampshire, USA (43.06N, 70.81W) to coincide with subtangent tracks of the Aura instruments. High-resolution (0.06 cm^{-1} FWHM) observed spectra are fit with calculated spectra to derive column and profile amounts of a number of atmospheric gases that also are measured by the Aura instruments. We concentrate here on comparisons with limb viewing measurements made by the Microwave Limb Sounder (MLS) [*Waters et al.*, 2006], High Resolution Dynamics Limb Sounder (HIRDLS) [*Gille et al.*, 2008] and Tropospheric Emission Spectrometer (TES) [*Beer*, 2006] experiments aboard Aura.

2. Observations

[3] The dynamics of the northern polar winter of 2004–2005 were such that a very cold and stable polar vortex was established which persisted throughout the period of the PAVE program. Furthermore the location of the vortex was such that the interior of the vortex was accessible within the flight range of the DC-8 from Pease airbase in Portsmouth, New Hampshire. The polar vortex exhibits a number of features that make it a suitable test for validation of satellite-borne sensors: it is a localized feature but large enough to easily locate; it has a relatively well understood structure; its location and movement are predictable; they occur on a regular basis in both hemispheres; some gases easily measured by satellite instruments increase within the vortex while some decrease; and polar vortices have sharp boundaries. All these features make the polar vortex a good target for testing the capabilities of satellite observations and retrieval techniques although they could serve to confound intercomparison activities.

[1] National Center for Atmospheric Research, Boulder, Colorado, USA.
[2] University of Denver, Denver, Colorado, USA.
[3] Clarendon Laboratory, University of Oxford, Oxford, UK.
[4] Jet Propulsion Laboratory, Pasadena, California, USA.

0148-0227/08/2007JD008833$09.00

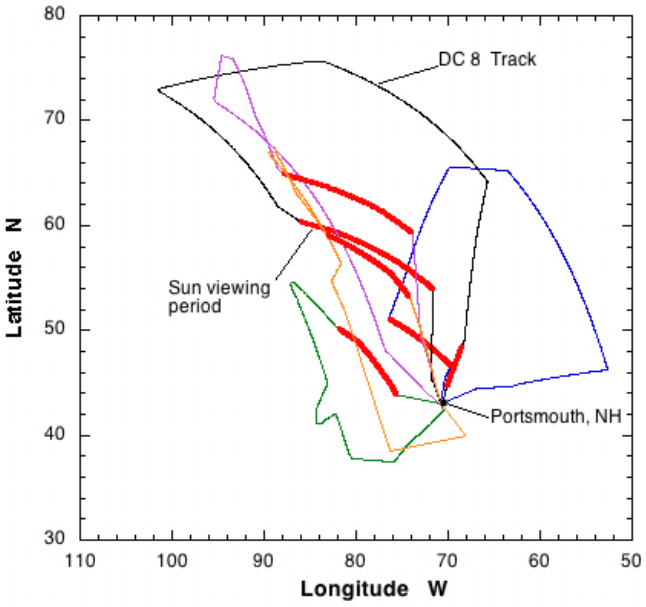

Date	Time (UT)	Latitude(N)
20050129	20:45-21:41 ss	53.3-59.3
20050131	20:00-20:58 ss	59.4-65.0
20050203	20:35-21:46 ss	43.0-52.3
20050205	12:39-13:17 sr	44.7-48.5
	20:00-21:11 ss	54.1-60.5
20050207	20:36-21:17 ss	46.8-50.8

Figure 1. DC-8 flight tracks during PAVE with segments highlighted that were suitable for viewing the sun by the NCAR FTS. Solar viewing periods typically were about an hour long. Note that sunrise (sr) and sunset (ss) were observed on 5 February 2005.

[4] Typical flights of the DC-8 during PAVE lasted for 8–10 h during which approximately one hour was devoted to tracking the setting sun for observations by the NCAR Fourier transform spectrometer (FTS). Figure 1 shows the DC-8 flight tracks out of Pease with an indication of the segment of each flight devoted to solar observing, denoted by highlighted portions of each flight track. The direction of observing is generally south from the aircraft and, for a typical solar elevation (5°) a ray from the sun passes through an altitude of 25 km at a distance of approximately 130 km from the aircraft. The six FTS observation periods, shown in Figure 1, were well distributed with respect to the polar vortex. Two flights were clearly outside the vortex, two within the transition region and one flight well within the interior of the vortex. Here we define the polar vortex as that region circumscribed by a maximum in the westerly wind at a level of about 20 km and identified by contours of Ertel Potential Vorticity (EPV) on the 50 mb surface as shown in Figure 2 (EPV analyses were provided by the NASA Ames Airborne Science Meteorological Support Team). The edge of the polar vortex, and the location of maximum wind, is closely associated with a value of 2.5×10^{-5} K m^2/kg s on the contours of Figure 2. Figures 2a–2e also show the 5 FTS observation tracks during PAVE on maps of EPV. We may consider the polar vortex to be a relatively conserved and stable entity that we were able to sample as it rotated about the pole; a reasonable assumption for the 9-day period of these observations. Figure 2f shows a schematic of the approximate locations of the 5 research flights with respect to the rotating vortex. The flight tracks in Figure 2f are displaced in a clockwise circumpolar direction, determined from trajectory analyses, to indicate the actual part of the vortex sampled. Trajectory analyses were performed using the NASA GSFC air parcel trajectory automailer [*Schoeberl and Sparling*, 1994].

3. Characterization of FTS Measurements

[5] Infrared spectra recorded by the NCAR FTS are simultaneously fit in one or more selected spectral regions for each gas of interest to retrieve the VMR vertical profiles using the optimal estimation technique employed in the SFIT2 retrieval code [*Chang and Shaw*, 1977; *Rinsland et al.*, 1982, 1998; *Connor et al.*, 1995, *Hase et al.*, 2004]. Table 1 shows the spectral regions used for each gas along with gases that have interfering absorption features in one or more of the regions. These interfering features also are fit by scaling the initial gas profile to minimize their effect on the target species retrieval. The retrieved VMR profile can be integrated to yield a vertical column from above the observation altitude to beyond the extent of the observation sensitivity. To remove possible differences due to aircraft altitude, calculation of partial column values given here begin at 13 km, just above the highest possible aircraft flight level.

[6] Fourier transformation and phase correction of the recorded interferograms and initial retrievals were performed in the field in near real time to provide initial science products. Each spectrum is composed of 10 interferogram scans of 16 cm that take 60 s integration time. The results given here were reanalyzed at a later time using appropriate temperature and pressure fields from curtain files derived by the NASA Ames Flight Support Team. Instrument function corrections derived from cell measurements [*Coffey et al.*, 1998] taken in flight after each solar observing period are used in the forward model [*Hase et al.*, 1999]. The measured instrument function remained essentially constant through the campaign. HITRAN 2004 line parameters [*Rothman et al.*, 2005] are used in the forward line-by-line spectral calculation. The forward model also includes solar absorption features [*Hase et al.*, 2006] adjusted with a single shift parameter that was fit in the retrieval process. Mixing ratio retrievals were constrained with a priori covariance described by the diagonal values and interlayer correlation lengths given in Table 1. Initial VMR profiles are given in Figure 3. These are derived from arctic balloon measurements [*Toon et al.*, 2002] except for H_2O. The water vapor profile is constructed from calculating a surface mixing ratio for a dew point 2°C below ambient falling to a nominal 4 ppm in the lower stratosphere.

[7] The NCAR FTS has been used for airborne measurements of this type for more than 25 years, and results, describing the latitudinal and seasonal dependences and time trends, of a number of upper tropospheric and stratospheric gases have been reported [*Coffey et al.*, 1981; *Mankin and Coffey*, 1983; *Coffey*, 1988; *Coffey et al.*,

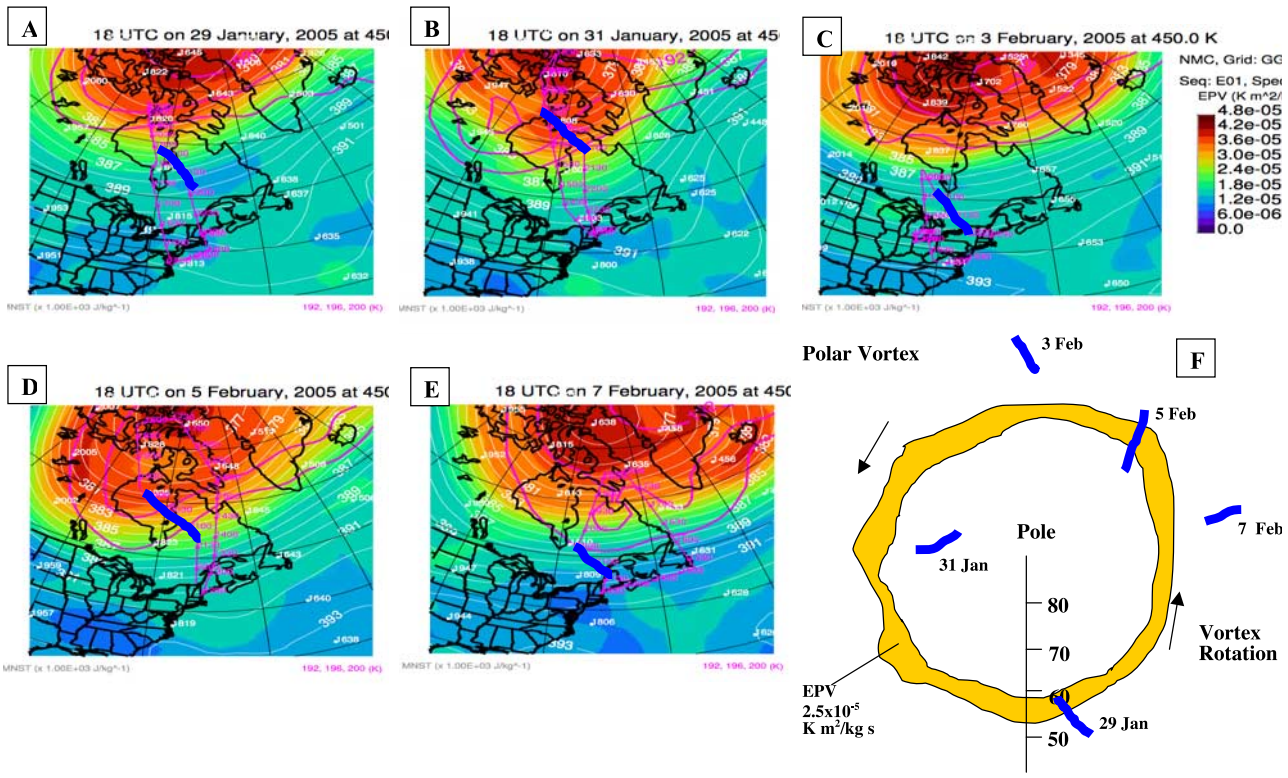

Figure 2. (a–e) Maps of Ertel potential vorticity at the 450 K surface along with DC-8 flight paths. Solar viewing periods are highlighted; view directions were generally southward. (f) A schematic of the five flights and their relative locations on a rotating vortex. The yellow region represents the collar region of the vortex and corresponds to the yellow contours in the maps of potential vorticity.

1989; *Mankin and Coffey*, 1989; *Coffey et al.*, 2006]. Recent upgrades to the optics and data system have improved the stability and signal-to-noise characteristics of the system. This along with advances in mixing ratio retrieval techniques for FTS's allow the retrieval of vertical profile information for several gases in the upper tropospheric to lower stratospheric region.

[8] Retrievals of mixing ratio profiles from a single line of sight measurement rely solely on the altitude-dependent

Table 1. Spectral and a Priori Parameters Used in the Optimal Estimation Retrievals[a]

Gas	Fit Regions, cm^{-1}	Interfering Species	SNR	A Priori Uncertainty	Interlayer Correlation
H_2O	2934.70–2935.70 2983.70–2984.70 2991.50–2992.50 2995.00–2996.00	CH_4, O_3, C_2H_4	300	5–70%	7 km
HCl	2821.30–2821.75 2925.60–2926.15 2944.50–2945.10	H_2O, N_2O, CH_4, HDO	300	20–50%	7 km
HF	4000.80–4001.20 4038.75–4039.20	H_2O	300	10–50%	7 km
HNO_3	867.50–871.80		200	50%	7 km
N_2O	2441.80–2444.40 2481.20–2482.50	CO_2, O_3	300	30–50%	7 km

[a]Spectral parameters include the fit regions and interfering species accounted for in those regions and the nominal SNR of the spectra. A priori parameters include the range of values of the diagonal elements of the VMR uncertainty and the half width of the Gaussian interlayer correlation length.

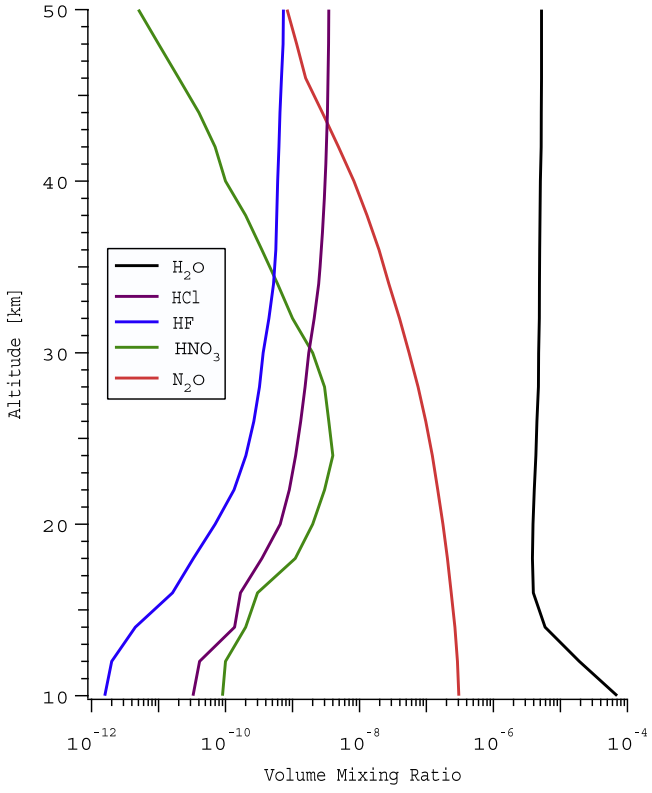

Figure 3. Initial VMR profiles for H_2O, HCl, HF, HNO_3, and N_2O.

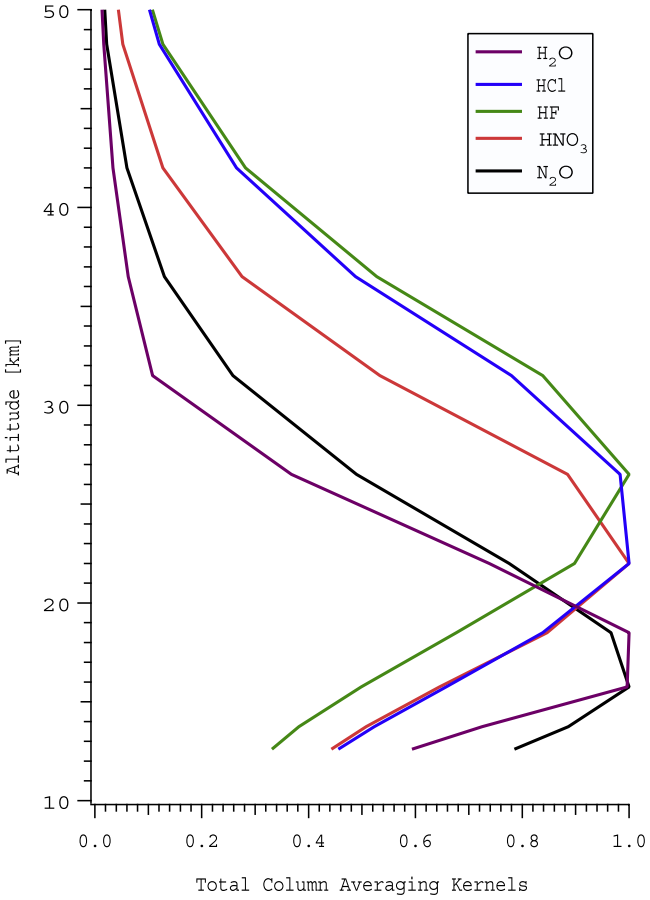

Figure 4. Total column-averaging kernels for each target gas calculated as the sum of the individual mixing ratio kernels.

pressure broadening effect on absorption by the target gas. The maximum altitude for information and vertical resolution are dependent on wavelength, spectral resolution of the FTS, signal-to-noise ratio (SNR) and the characterization of the instrument line shape (ILS). In the infrared spectral region, where our measurements are made, retrievals may be made up to about 30 km, depending on the gas, as illustrated in Figure 4. The information retrieved using the OE technique can be illustrated by the degrees of freedom for signal (DOFS) that are given in Table 2 and the total column-averaging kernels that are shown in Figure 4. The DOFS show that between 1 and 2 independent pieces of information distributed in the retrieved profile are available for this data set dependent on the species. The altitude range of the information is near the kernel peaks shown in Figure 4 and also varies with species. Where the kernels fall to 0.5 and below the retrieved profile is composed chiefly of the a priori.

[9] Uncertainty in the column retrieval, due predominantly to random and systematic sources, are given in Table 3. Sensitivity calculations used to generate these uncertainties were performed on the retrieval altitude grid and altitude-dependent error values were derived. Air-broadening coefficient, line strength and ILS are considered systematic uncertainties. Uncertainty in line strengths have been taken from the HITRAN 2004 database, air-broadening coefficient

Table 2. Results of the Uncertainty Analysis for Total Column Values for Each Gas[a]

Gas	Sum Systematic	Sum Random	Total	DOFS
H_2O	4.13%	4.11%	8.25%	1.8
HCl	3.79%	7.86%	11.65%	1.6
HF	2.67%	7.10%	9.76%	1.3
HNO_3	8.04%	7.41%	15.45%	1.4
N_2O	3.47%	3.61%	7.08%	1.9

[a]These are the RSS of the random and systematic values, and their sum gives the total uncertainty. The degrees of freedom for signal is calculated as the rank of the averaging kernel matrix.

uncertainty is taken to be 5%. Owing to the stability of the ILS, the estimate in its uncertainty of 5% is determined to have a systematic effect on the data set. Random uncertainties are composed of a pointing deviation of 0.1° from the calculated solar zenith angle. Consideration has been made for the fact that zenith angle time is based on the time recorded from the real-time on-board DADS data stream that could differ from the data acquisition computer time. Solar tracking is performed by a stable two-axis dynamic tracker fixed on the FTS frame. An estimate of 2°C from the nominal temperature profile was used to calculate sensitivities of total column and mixing ratio uncertainties. The temperature profile used was an average of all temperature profiles provided by the NASA Ames Support Team during a given sun run typically 30–50 profiles. Estimation of uncertainty includes the effect on the air mass and ray tracing as well as partition function and line strength calculations. The random measurement error shows the uncertainty in the column due to the finite SNR of the measurement. The effect of the uncorrelated measurement covariance on the retrieved profile in the OE formulation is given by

$$S_m = D_y S_\varepsilon D_y^T,$$

where D_y is the contribution function or sensitivity of the retrieval to the measurement [*Rodgers*, 1990] and S_ε is the measurement covariance.

[10] The resultant uncertainty in random and systematic components and their sum is given in Table 2. Measurement error tends to dominate the budget except for HNO_3 where uncertainty in laboratory derived line strengths of 8% is predominant. Smoothing error that describes an inherent mismatch between a retrieved profile and the actual profile due to the vertical resolution of the measurement technique is not included here as an uncertainty component. Each measurement technique described here has an associated smoothing error that is described in their averaging kernel

Table 3. Components of the Uncertainty in Total Column for Each Target Gas

Gas	Air-Broadened Coefficient	ILS	Line Strength	Pointing	Temperature	Measurement
H_2O	0.56%	0.97%	3.98%	1.53%	0.60%	3.77%
HCl	0.30%	2.44%	2.88%	1.11%	1.15%	7.70%
HF	0.28%	1.81%	1.94%	1.00%	1.42%	6.88%
HNO_3	0.75%	1.08%	7.93%	1.41%	1.85%	7.04%
N_2O	0.59%	1.68%	2.98%	1.36%	0.50%	3.31%

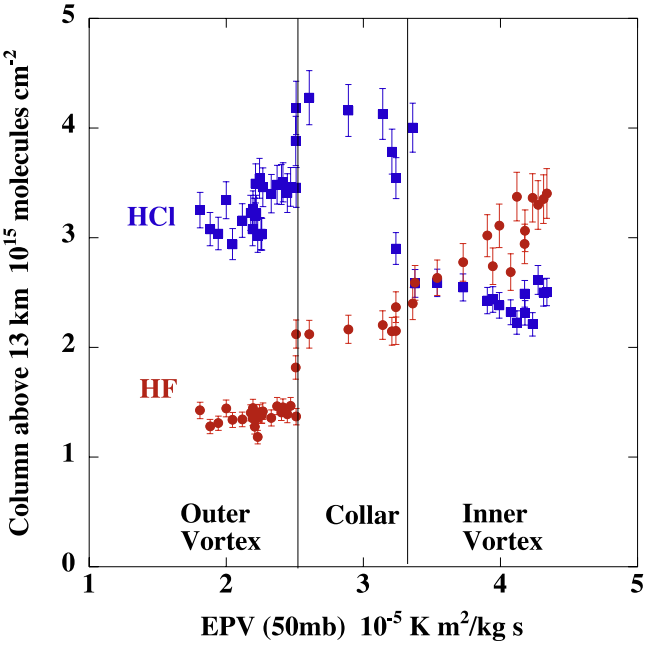

Figure 5. Column amounts of HCl and HF versus potential vorticity showing the change in dynamics and chemistry in the vicinity of the polar vortex.

matrix. While it is possible to use the averaging kernels from each approach to aid in the comparison, by removing the inherent smoothing of each technique, the current error assumptions of the FTS, MLS, TES and HIRDLS seem sufficient for this comparison. Plots comparing profiles retrieved from the different sounders show errors associated with the measurement and retrieval.

4. Results

[11] Figure 5 shows column amounts derived from FTS observations of HCl and HF versus EPV (50 mb) for the PAVE period. To translate to vortex-centered space we assign to each observation the EPV at 50 mb as calculated by the Goddard Space Flight Center (GSFC) PAVE Science support team and provided as a curtain of data that follows the DC-8 flight track (XS files in the PAVE archive). As indicated in the figure the measurements at EPV $< \sim 2.5 \times 10^{-5}$ K m^2/kg s are generally outside the influence of the polar vortex and represent typical midlatitude values of HCl and HF that produce an HCl/HF ratio near 2. Measurements between EPV = 2.5 and 3.5 $\times$ 10^{-5} K m^2/kg s indicate strong descent within the collar region of the vortex, descent that increases the column amounts of both HCl and HF as air rich in HCl and HF from higher altitudes is transported to lower altitudes (and replaced at the upper levels by equally rich air). Within the vortex we see the combined effect of descent (that increases HCl and HF) and chemical destruction (that affects only HCl). Deeper within the vortex Figure 5 shows the destruction of HCl relative to the still increasing HF amount. These observations are consistent with current understanding of polar processes [*Newman and Rex*, 2007] and indicate a well established cold polar vortex. The NH wintertime polar vortex of 2004–2005 was the coldest and most extensive of record with a potential for Polar Stratospheric Cloud (PSC) formation on more days and over a larger area than in any previous year [*Manney et al.*, 2006]. The PAVE mission was fortunate to be able to sample the polar vortex so well with a limited number of flights from a relatively low latitude base.

[12] Flights of the DC-8 were designed to coincide with overpasses of the Aura satellite which, due to its 98 degree inclination orbit, generally are in a north-south direction. However, the solar observing periods of the DC-8 flights are generally more west-to-east to allow tracking the low elevation sun through an infrared transmitting window in the right side of the aircraft. Locations of the FTS, HIRDLS, MLS and TES observations on each of the 5 solar flights are shown in Figure 6. HIRDLS and MLS are limb-viewing instruments aboard Aura and made observations in the vicinity of the DC8 flight track on each of the 5 FTS solar-observing days. TES, which normally has a nadir viewing geometry, also may be utilized in a limb-viewing mode as was done on two days (29 and 31 January 2005) to produce HNO_3 vertical profiles. Also indicated in Figure 6 are the times of observation. For the intercomparisons shown here locations are selected to be within about 600 km and within 3 h. Regions of intercomparison between the aircraft and satellite observations are shown as shaded portions of Figure 6. As may be seen these regions are largely either inside or outside the polar vortex, as defined by the 2.5 $\times$ 10^{-5} K m^2/kg s PV contour, that also is shown in the figure. This situation is further supported by the relatively small variation in constituents, such as HNO_3, measured by the aircraft or satellite instruments within the comparison regions. This is indicated in Figure 7 by the standard deviations of the observed HNO_3.

[13] Figure 7 shows vertical profiles for HNO_3 derived from NCAR FTS measurements, HIRDLS version 2.04.08, MLS version 2.20 and TES version V003 analyses. The average of mixing ratio vertical profiles for observations contained within the shaded areas of Figure 6 are shown in Figure 7 along with estimated uncertainties in those profiles. There are typically between 5 and 12 individual profiles in each average profile shown in Figure 7 as indicated by the symbols inside the blue shaded box of Figure 6. The upper altitude (lower pressure) of Figure 7 is cut off when the a priori begins to dominate the measurement, above about 10 hPa. As seen in Figure 7 there is relatively good agreement among the various observations of HNO_3 except that the retrieval from the aircraft observations suggests a layer of enhanced HNO_3 on days when observations were made within or near the boundary of the polar vortex (20050129, 20050131 and 20050205). On the other two days, outside the vortex, there is good agreement between the aircraft and satellite observations. Figure 8 shows column amounts of HNO_3 above an altitude of 13 km versus latitude for the same days as Figure 7. FTS results are indicated by solid symbols in Figure 8 and MLS results are corresponding open symbols. Errors, shown in Figure 8, for FTS measurements are from the error simulations described above and represent typically 15%, for MLS error bars are 10% as recommended in the MLS data quality document [*Livesey et al.*, 2005] (and Version 2.20 updates, November 2006). Error estimates for HIRDLS are contained in the HIRDLS Data Description and Quality document [*Gille*

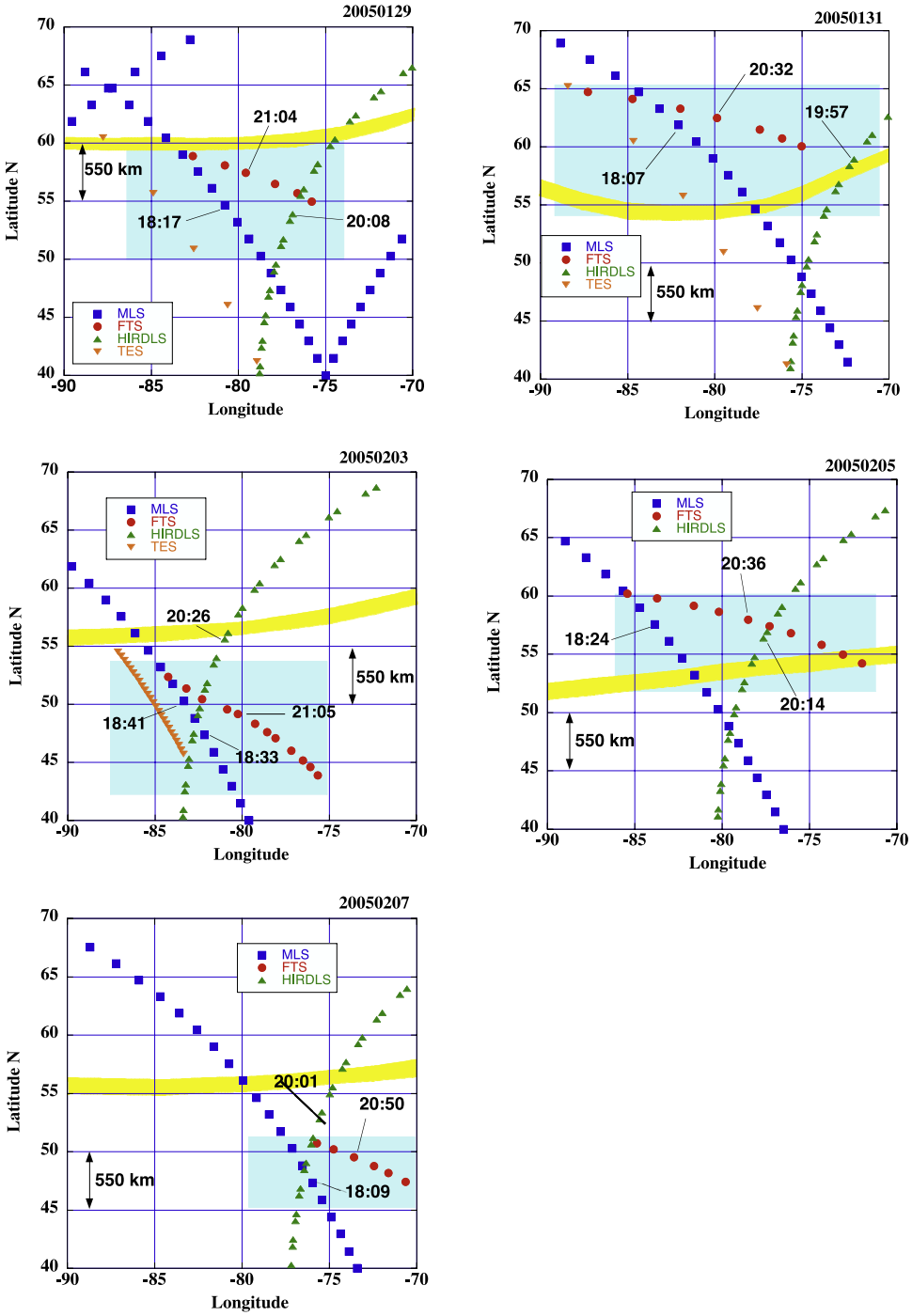

Figure 6. Maps of NCAR FTS observation locations with subtangent points for observations by HIRDLS, MLS, and TES at nearly coincident times. Satellite crossing times are similar each day for a given location. Also shown are approximate polar vortex boundaries as defined in the text. Data within the shaded areas are used for subsequent plots.

and Barnett, 2006] and for TES in the TES Level 2 Data User's Guide [*Osterman et al.*, 2006]. As may be seen in Figure 8, HNO_3 column amounts generally agree to within the overlap of the errors except for 31 January 2005. It also is clear in Figure 8 that, regarding HNO_3, the observations on 29 January 2005 were more like inner vortex air than outer vortex. The mean difference between adjacent observations by MLS and the FTS is 2.4%, (1.8% if 31 January is not included). On 31 January the views of the aircraft and Aura-borne instruments would have been through a part of the polar vortex characterized by relatively sharp gradients as may be seen in Figure 2b. The MLS line-of-sight (LOS) is in the direction of spacecraft motion while HIRDLS and TES (limb mode) view a number of degrees off the spacecraft track aft of the direction of flight. A feature of any satellite-borne limb-viewing instrument will be the

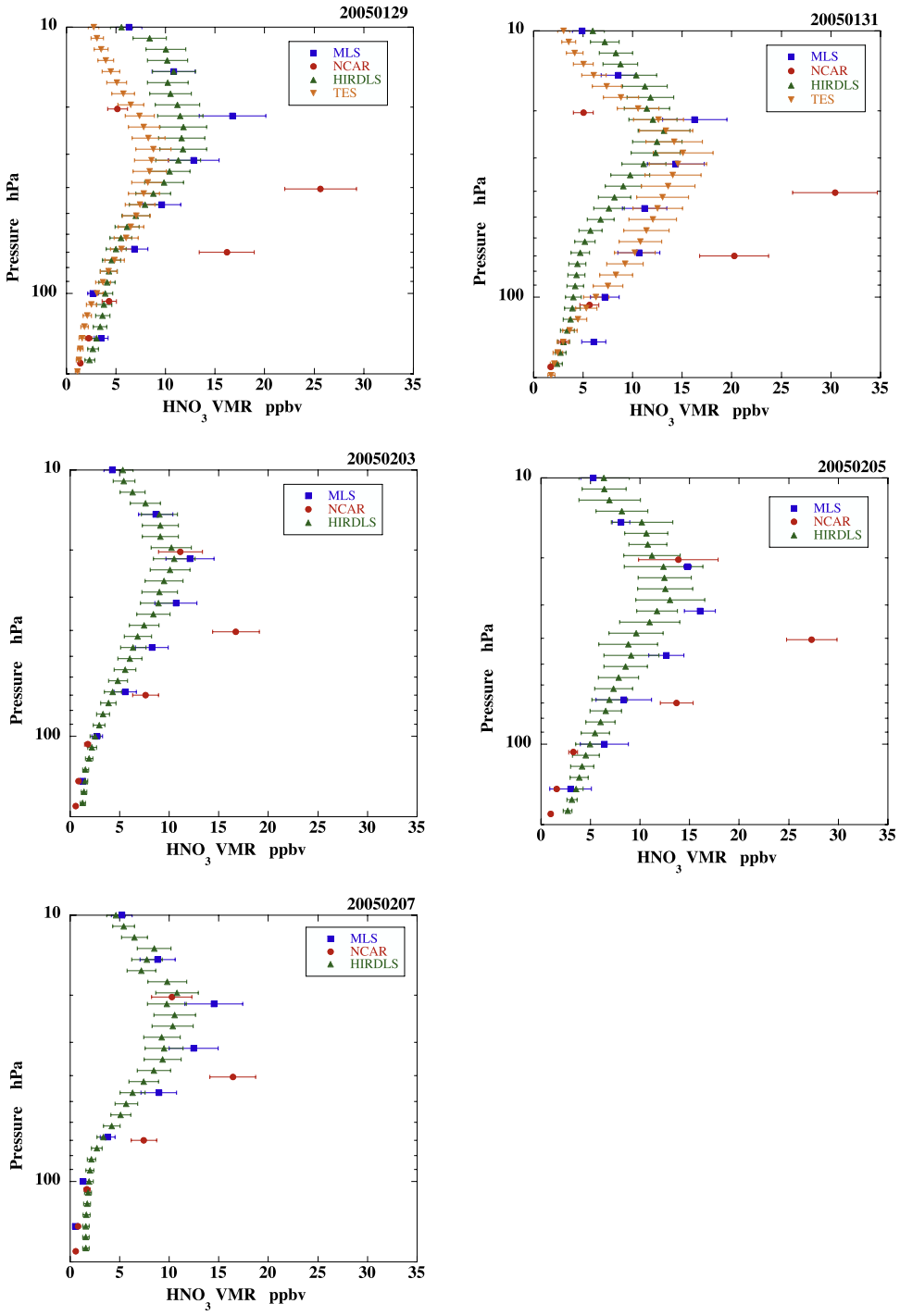

Figure 7. Vertical profiles of HNO_3 average mixing ratio from HIRDLS, MLS, TES, and the NCAR FTS. Error bars represent estimated uncertainties for an individual VMR profile.

relatively large horizontal averaging of the measurement compared to the horizontal extent of the aircraft FTS LOS. If there are large horizontal gradients in HNO_3 this may account for the differences in retrieved HNO_3 columns, and differences in other gases discussed below, when the aircraft and satellite views are through the steepest gradients near the vortex boundary. The vertical resolution of the FTS retrieval is not optimum to locate a thin layer in the profile of HNO_3, as discussed earlier, and the maxima in the FTS profiles for 20050129, 20050131 and 20050205 are probably an overestimate. However, the implication of the retrievals, based on a number of solid fits of very good spectra, for those three days within the vortex, is that there is a layer of enhanced HNO_3 at altitudes near 18 km with perhaps some depletion of HNO_3 above. This situation is supported by HNO_3 observations by the submillimeter

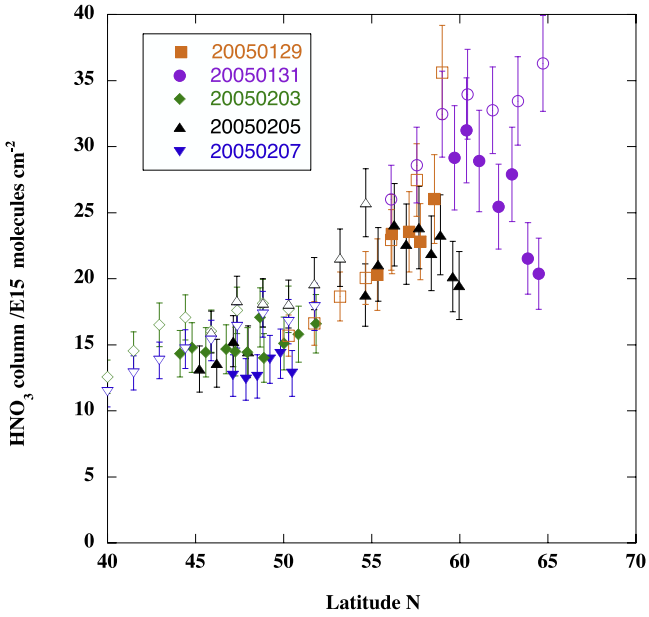

Figure 8. Column amounts of HNO_3 above 13 km versus latitude for all 5 days of PAVE observation. Solid symbols represent FTS observations; corresponding open symbols are MLS results. Error bars are the uncertainties in the results as described in the text.

emission radiometer (ASUR), also flown on the DC-8 during PAVE, that reported HNO_3 maxima greater than 13 ppbv near 16 km altitude and minima below 4 ppbv near 22 km. They attributed this to a redistribution of HNO_3 by sedimentation (and reevaporation) of nitric acid particles [*Kleinböhl et al.*, 2005].

[14] Figure 9 shows columns of HCl measured by the NCAR FTS and MLS on Aura for the five observation days. As for HNO_3 there is generally good agreement except for day 20050131 where the MLS columns show less HCl than the FTS results. The average difference between adjacent observations is 4.6%. The error bars on the FTS HCl observations are from the full error analysis and represent about 11%. The larger differences on day 20050131 may be due to sharp gradients in HCl (and HNO_3) near the edge of the polar vortex.

[15] Figure 10 shows N_2O mixing ratio vertical profiles measured by the NCAR FTS and MLS and HIRDLS on Aura. Error bars are plus and minus 20% for the Aura observations and are the estimated systematic plus random error for the FTS observations.

[16] Figure 11 shows VMR results for H_2O from the NCAR FTS and MLS with generally good agreement. The relatively good comparisons between the airborne FTS and MLS and HIRDLS for N_2O and H_2O show that the vertical profiles of these gases may not be as disturbed by the influence of the polar vortex. We recognize that the vertical averaging kernels of the various satellite and aircraft techniques may not be perfectly matched and may limit the applicability of intercomparisons [*Rodgers and Connor*, 2003], as discussed earlier. We would point out that column amounts derived from satellite and aircraft observations offer the most appropriate quantities for comparison [*Rodgers and Connor*, 2003], and we have shown a sample here.

5. Summary

[17] Nearly coincident observations of HNO_3, HCl, N_2O and H_2O in the vicinity of the northern polar vortex in January and February 2005 have shown reasonably good agreement between an aircraft-borne infrared spectrometer and the HIRDLS, MLS and TES instruments aboard the EOS Aura satellite. Observations by the airborne and satellite instruments usually were made within about 600 km and 3 h of each other. Mixing ratio profile and column results show that the best agreement among all the techniques is found on days when the constituent fields are not disturbed by the dynamics and chemical processing of the polar vortex. Days 20050203 (3 February 2005) and 20050207 (7 February 2005) were least influenced by the vortex, the mean difference in column amounts derived by MLS and the FTS on those days was 4.6% for HCl and 2.4% for HNO_3. Largest differences occur on days when observations were made in a region of the vortex with large gradients in wind and potential vorticity, differences were especially noticeable in results for HNO_3 and HCl whose profiles may be dramatically changed by vortex activity. Nitric acid profile results from the three satellite instruments (results were not available for all days) generally had overlapping standard deviations while the aircraft FTS retrieval shows a layer of enhanced HNO_3 on days believed to be influenced by the polar vortex. N_2O shows reasonable good agreement between all the techniques with a small positive bias in the HIRDLS observation. Water vapor results were consistent between MLS and the FTS except on one day at the lowest altitude of the retrieval. Differences between aircraft and satellite observations may be due to their respective lines-of-sight through high-gradient regions

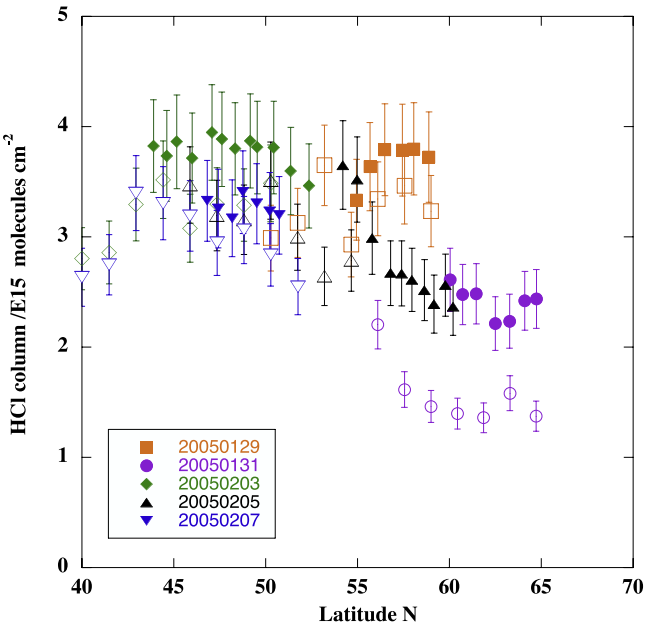

Figure 9. Column amounts of HCl above 13 km from the FTS and MLS. Symbols are as in Figure 8.

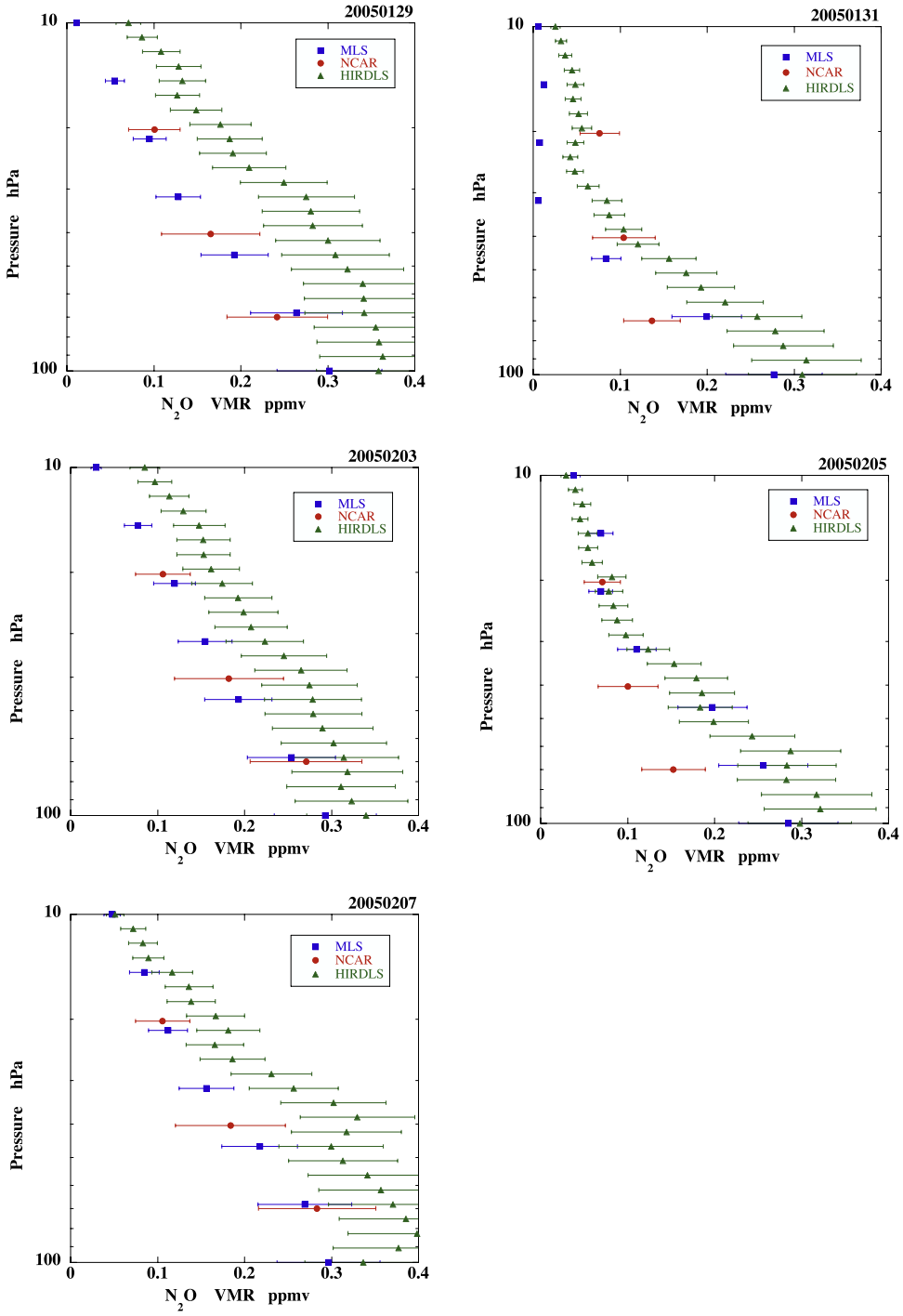

Figure 10. Vertical profiles of N_2O VMR for HIRDLS, MLS and the NCAR FTS. Errors as in Figure 7.

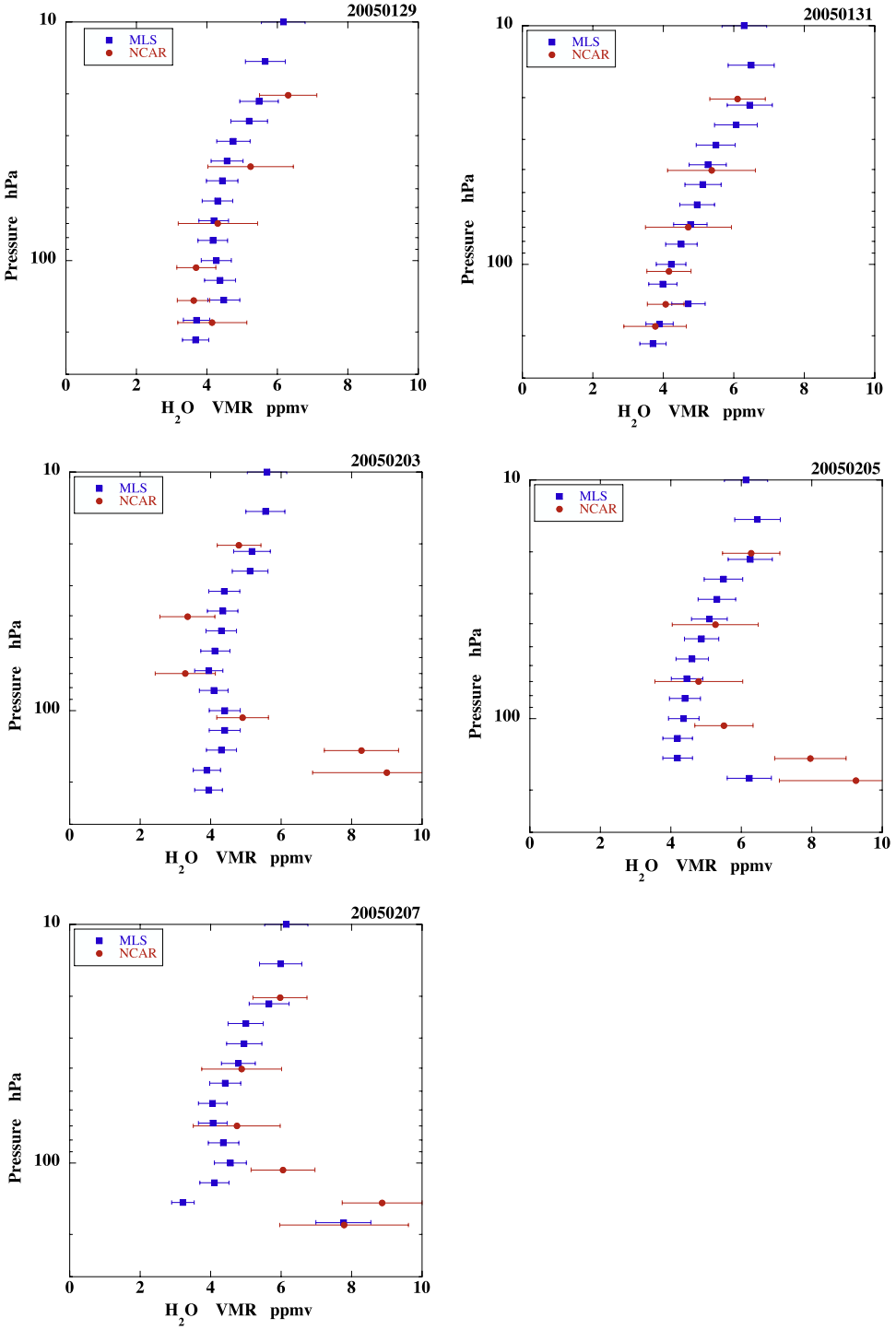

Figure 11. Vertical profiles of H_2O VMR as in Figures 7 and 10.

of the vortex. Observations of the polar vortex, in either hemisphere, could be a good test of the ability of satellite limb-viewing instruments to resolve sharp gradients in constituent amounts in both the horizontal and vertical. This intercomparison has demonstrated some of the capabilities of the new Aura satellite instruments relative to the established FTS observations, however, a statistical intercomparison would require more than 5 days of overlap.

[18] **Acknowledgments.** We would like to acknowledge the excellent support of the DC-8 technical and flight teams and the NASA GSFC management that made the PAVE possible. Work involving HIRDLS measurement and analysis is supported through contract NAS5–97046. The National Center for Atmospheric Research is supported by the National Science Foundation. Work at the Jet Propulsion Laboratory, California Institute of Technology, was carried out under a contract with the National Aeronautics and Space Administration.

References

Beer, R. (2006), TES on the Aura mission: Scientific objectives, measurements, and analysis overview, *IEEE Trans. Geosci. Remote Sens.*, *44*, 1102–1105, doi:10.1109/TGRS.2005.863716.

Chang, Y. S., and J. H. Shaw (1977), A nonlinear least squares method of determining line intensities and half-widths, *Appl. Spectrosc.*, *31*, 213–220, doi:10.1366/000370277774463760.

Coffey, M. T. (1988), On the Temporal Change of Stratospheric NO_2, *Geophys. Res. Lett.*, *15*, 331–334, doi:10.1029/GL015i004p00331.

Coffey, M. T., W. G. Mankin, and A. Goldman (1981), Simultaneous spectroscopic determination of the latitudinal, seasonal and diurnal variability of stratospheric N_2O, NO, NO_2, and HNO_3, *J. Geophys. Res.*, *86*, 7331–7341, doi:10.1029/JC086iC08p07331.

Coffey, M. T., W. G. Mankin, and A. Goldman (1989), Airborne measurements of stratospheric constituents over Antarctica in the austral spring 1987: 2. Halogen and nitrogen trace gases, *J. Geophys. Res.*, *94*, 16,597–16,614, doi:10.1029/JD094iD14p16597.

Coffey, M. T., A. Goldman, J. W. Hannigan, W. G. Mankin, W. G. Schoenfeld, C. P. Rinsland, C. Bernardo, and D. W. T. Griffith (1998), Improved vibration-rotation (0–1) HBr line parameters for validating high resolution infrared atmospheric spectra measurements, *J. Quant. Spectrosc. Radiat. Transfer*, *60*, 863–867, doi:10.1016/S0022-4073(98)00088-0.

Coffey, M. T., J. W. Hannigan, and A. Goldman (2006), Observations of upper tropospheric/lower stratospheric water vapor and its isotopes, *J. Geophys. Res.*, *111*, D14313, doi:10.1029/2005JD006093.

Connor, B. J., A. Parrish, J. J. Tsou, and M. P. McCormick (1995), Error analysis for the ground-based microwave ozone measurements during STOIC, *J. Geophys. Res.*, *100*, 9283–9291, doi:10.1029/94JD00413.

Gille, J. C., and J. J. Barnett (2006), HIRDLS Data description and quality, version 2.0, SC-HIR-1511, Natl. Cent. for Atmos. Res., Boulder, Colo.

Gille, J., et al. (2008), The High Resolution Dynamics Limb Sounder (HIRDLS): Experiment overview, recovery, and validation of initial temperature data, *J. Geophys. Res.*, doi:10.1029/2007JD008824, in press.

Hase, F., T. Blumenstock, and C. Paton-Walsh (1999), Analysis of the instrumental line shape of high-resolution Fourier transform IR spectrometers with gas cell measurements and a new retrieval software, *Appl. Opt.*, *38*(15), 3417–3422.

Hase, F., J. W. Hannigan, M. T. Coffey, A. Goldman, M. Hopfner, N. B. Jones, C. P. Rinsland, and S. W. Wood (2004), Intercomparison of retrieval codes used for the analysis of high-resolution, ground-based FTIR measurements, *J. Quant. Spectrosc. Radiat. Transfer*, *87*, 25–52, doi:10.1016/j.jqsrt.2003.12.008.

Hase, F., P. Demoulin, A. J. Sauval, G. C. Toon, P. F. Bernath, A. Goldman, J. W. Hannigan, and C. P. Rinsland (2006), An empirical line-by-line model for the infrared solar transmittance spectrum from 700 to 5000 cm^{-1}, *J. Quant. Spectrosc. Radiat. Transfer*, *102*, 450–463.

Kleinböhl, A., H. Bremer, H. Küllmann, J. Kuttippurath, E. V. Browell, T. Canty, R. J. Salawitch, G. C. Toon, and J. Notholt (2005), Denitrification in the Arctic mid-winter 2004/2005 observed by airborne submillimeter radiometry, *Geophys. Res. Lett.*, *32*, L19811, doi:10.1029/2005GL023408.

Livesey, N. J., et al. (2005), Earth Observing System, Microwave Limb Sounder, version 1.5 Level 2 data quality and description document, *JPL D-32381*, July.

Mankin, W. G., and M. T. Coffey (1983), Latitudinal distribution and temporal changes of stratospheric HCl and HF, *J. Geophys. Res.*, *88*, 10,776–10,784, doi:10.1029/JC088iC15p10776.

Mankin, W. G., and M. T. Coffey (1989), Airborne measurements of stratospheric constituents over Antarctica in the austral spring 1987: 1. Method and ozone observations, *J. Geophys. Res.*, *94*, 11,413–11,421, doi:10.1029/JD094iD09p11413.

Manney, G. L., M. L. Santee, L. Froidevaux, K. Hoppel, N. J. Livesey, and J. W. Waters (2006), EOS MLS observations of ozone loss in the 2004–2005 Arctic winter, *Geophys. Res. Lett.*, *33*, L04802, doi:10.1029/2005GL024494.

Newman, P. A., and M. Rex (2007), Polar ozone: Past and present, in *Scientific Assessment of Ozone Depletion: 2006, Global Ozone Res. and Monit. Proj. Rep.* 50, 572 pp. 4/1–4.37, World Meteorol. Org., Geneva.

Osterman, G., et al. (2006) *TES L2 Data User's Guide, Version 2.0*, Jet Propul. Lab., Pasadena, Calif.

Rinsland, C. P., M. A. H. Smith, P. L. Rinsland, A. Goldman, J. W. Brault, and G. M. Stokes (1982), Ground-based infrared spectroscopic measurements of atmospheric hydrogen cyanide, *J. Geophys. Res.*, *87*, 11,119–11,125, doi:10.1029/JC087iC13p11119.

Rinsland, C. P., et al. (1998), Northern and Southern Hemisphere ground-based infrared spectroscopic measurements of tropospheric carbon monoxide and ethane, *J. Geophys. Res.*, *103*, 28,197–28,217, doi:10.1029/98JD02515.

Rodgers, C. D. (1990), Characterization and error analysis of profiles retrieved from remote sounding measurements, *J. Geophys. Res.*, *95*, 5587–5595, doi:10.1029/JD095iD05p05587.

Rodgers, C. D., and B. J. Connor (2003), Intercomparison of remote sounding instruments, *J. Geophys. Res.*, *108*(D3), 4116, doi:10.1029/2002JD002299.

Rothman, L. S., et al. (2005), The HITRAN 2004 molecular spectroscopic database, *J. Quant. Spectrosc. Radiat. Transfer*, *96*, 139–204, doi:10.1016/j.jqsrt.2004.10.008.

Schoeberl, M. R., and L. C. Sparling (1994), Trajectory modelling, in Diagnostic Tools in Atmospheric Physics, edited by G. Fiocco and G. Visconti, North-Holland, Amsterdam.

Toon, G. C., B. Sen, J. F. Blavier, Y. Sasano, T. Yokota, H. Kanzawa, T. Ogawa, M. Suzuki, and K. Shibasaki (2002), Comparison of ILAS and MkIV profiles of atmospheric trace gases measured above Alaska in May 1997, *J. Geophys. Res.*, *107*(D24), 8211, doi:10.1029/2001JD000640.

Waters, J. W., et al. (2006), The Earth Observing System Microwave Limb Sounder (EOS MLS) on the Aura satellite, *IEEE Trans. Geosci. Remote Sens.*, *44*, 1075–1092, doi:10.1109/TGRS.2006.873771.

M. T. Coffey, J. C. Gille, J. W. Hannigan, and D. Kinnison, National Center for Atmospheric Research, P.O. Box 3000, Boulder, CO 80307, USA. (coffey@ucar.edu)

J. J. Barnett, Clarendon Laboratory, University of Oxford, Parks Road, Oxford OX1 3PU, UK.

R. Beer, B. Fisher, L. Froidevaux, S. S. Kulawik, A. Lambert, N. Livesey, and M. Santee, Jet Propulsion Laboratory, 4800 Oak Grove Drive, Pasadena, CA 91109-8099, USA.

A. Goldman, University of Denver, 2112 E. Wesley Avenue, Denver, CO 80208, USA.